Journal of Molecular Structure 1198 (2019) 126888

Contents lists available at ScienceDirect

Journal of Molecular Structure

journal homepage: http://www.elsevier.com/locate/molstruc

Synthesis, characterisation and biological studies of mixed-ligand nickel (II) complexes containing imidazole derivatives and thiosemicarbazide Schiff bases

Nurul N.M. Ishak [a], Junita Jamsari [a], A.Z. Ismail [a], Mohamed I.M. Tahir [a], Edward R.T. Tiekink [b], Abhi Veerakumarasivam [c, d], Thahira B.S.A. Ravoof [a, e, *]

[a] Department of Chemistry, Faculty of Science, Universiti Putra Malaysia, 43400, UPM Serdang, Selangor Darul Ehsan, Malaysia
[b] Research Centre for Crystalline Materials, School of Science and Technology, Sunway University, No. 5 Jalan Universiti, 47500, Bandar Sunway, Selangor Darul Ehsan, Malaysia
[c] Department of Biological Sciences, School of Science and Technology, Sunway University, No. 5 Jalan Universiti, 47500, Bandar Sunway, Selangor Darul Ehsan, Malaysia
[d] Medical Genetics Laboratory, Faculty of Medicine and Health Sciences, Universiti Putra Malaysia, 43400, UPM Serdang, Selangor Darul Ehsan, Malaysia
[e] Materials Synthesis and Characterization Laboratory, Institute of Advanced Technology, Universiti Putra Malaysia, 43400, UPM Serdang, Selangor Darul Ehsan, Malaysia

ARTICLE INFO

Article history:
Received 1 June 2019
Received in revised form
16 July 2019
Accepted 31 July 2019
Available online 7 August 2019

Keywords:
Mixed-ligand complexes
Single Crystal X-ray diffraction
Imidazole
Thiosemicarbazone
Schiff base

ABSTRACT

Four new mixed-ligand Ni(II) complexes (**1**–**4**) containing imidazole (im) or benzimidazole (bz) and tridentate Schiff bases derived from 2,4-dihydroxybenzaldehyde (24D) and 4-methyl-3-thiosemicarbazide (MT24D) or 4-phenyl-3-thiosemicarbazide (PT24D) were synthesised and characterised using elemental and spectral analysis including FTIR, UV–Vis, ^{1}H NMR, ^{13}C NMR and mass spectrometry for Schiff bases, while the complexes were additionally analysed using ICP-OES, molar conductivity, magnetic susceptibility measurements and single crystal X-Ray diffraction (SXRD) analysis. Magnetic susceptibility indicated a square planar geometry for all the metal complexes while molar conductance values showed that the complexes were non-electrolytes in DMSO. The molecular geometries of the neutral complex molecule in [Ni(MT24D)(bz)](bz).CH_3OH (**2′**), that is **2** co-crystallised with a 1,3-benzimidazole molecule as a methanol solvate, and in the cation of [Ni(MT24D)(im)]O_2CMe.$2H_2O$ (**5**), a reaction intermediate for **1**, were established by X-ray crystallography. Each featured a trans-N_2OS coordination geometry defined by phenoxide-O, imine-N and thiolate-S (**2′**) or thione-S (**5**) donors as well as the imine-N donors derived from 1,3-benzimidazole (**2′**) or imidazole (**5**) molecules. Systematic variations in geometric parameters were correlated with the form of the tridentate ligand, i.e. di-anionic (**2′**) or mono-anionic (**5**). In the crystal of **2′**, supramolecular chains were sustained by hydrogen bonding and these were connected into a supramolecular layer by π ··· π stacking interactions occurring between coordinated benzimidazole rings. In the crystal of **5**, hydrogen bonding led to a three-dimensional architecture. The Schiff bases and mixed-ligand Ni(II) complexes were tested for their cytotoxic activitY, but all compounds were inactive against the MDA-MB-231 and MCF-7 breast cancer cell lines. Interestingly, the antibacterial analysis of the compounds showed that the PT24D Schiff base, Ni(MT24D)im, Ni(MT24D)bz, and Ni(PT24D)bz complexes had specific and selective activity against *Staphylococcus aureus (S. aureus), Bacillus subtilis (B. subtilis), Propionibacterium acne (P. acne) and Enterobacteraerogenes (E. aerogenes).* The DNA binding studies of mixed-ligand Ni(II) complexes against calf thymus DNA revealed that slight hypochromism was observed in the absorption spectra suggesting π-π interactions between the aromatic chromophores and the DNA base pairs where **2** had higher K_b values than **1** thus indicating stronger interactions.

© 2019 Elsevier B.V. All rights reserved.

1. Introduction

In recent years, multi-drug resistance has become a serious

* Corresponding author. Department of Chemistry, Faculty of Science, Universiti Putra Malaysia, 43400, UPM Serdang, Selangor Darul Ehsan, Malaysia.
E-mail address: thahira@upm.edu.my (T.B.S.A. Ravoof).

https://doi.org/10.1016/j.molstruc.2019.126888
0022-2860/© 2019 Elsevier B.V. All rights reserved.

issue resulting in significant morbidity and mortality. Thus, there is a need to develop new types of drugs that can overcome this growing problem. Transition metal complexes as metallo-drugs are believed to have great potential as anti-microbial agents [1,2]. Small molecules like transition metal complexes have been proven to have strong binding interactions with DNA via both covalent and non-covalent interaction modes. The interaction modes play a significant role in the biological activities of metal complexes especially as antibacterial, antifungal and anticancer agents [3]. For example, the Cu(II) Schiff base complex derived from 4-chloroanthranilic and salicylaldehyde showed an intercalative binding mode with CT-DNA with a high K_b constant of 1.93×10^4 L mol^{-1}, indicative of strong binding, as compared to other similar complexes such as [Cu(naph-leu)phen] $CH_3OH \cdot 0.5H_2O$ (K_b, 4.87×10^3 L mol^{-1}) and [Cu(sal-L-val)phen] (K_b, 6.48×10^3 L mol^{-1}) [4]. This has formed the basis of most research in the synthesis of metal complexes via various methods and different designs to develop new metal-based drugs.

Transition metal complexes of thiosemicarbazone ligands have received considerable interest due to its ability to disrupt DNA synthesis by causing modification in the reductive conversion of ribonucleotides to deoxyribonucleotides [5]. Furthermore, by introducing aldehydes or ketones to thiosemicarbazones, the Schiff bases that are formed can interact with metal ions to form complexes that have stable four, five or six coordination [6,7]. The biological activity of thiosemicarbazones is facilitated by their chelating ability with transition metal ions. Coordination to metal centre through sulphur and nitrogen donors would form bidentate, tridentate or even multidentate ligands, thus giving rise to complexes of different geometries and properties that would alter or enhancing their biological properties [8–12]. Studies also reported that the biological activity of the metal complexes of thiosemicarbazone-derived Schiff bases often had higher, and selective bioactivities as compared to the corresponding free thiosemicarbazones [13–15]. The biological activity of these metal complexes containing Schiff bases have also been reported to have enhanced activities when ligated to a co-ligand, forming mixed-ligand complexes. For instance, the Cu(II) complexes of a tridentate Schiff base, salicylaldehyde-4-methyl-3-thiosemicarbazone in the presence of imidazole or benzimidazole exhibited enhanced activity against MCF-7 and MDA-MD-231 breast cancer cell lines [16] as compared to the mono-ligand metal complex.

Imidazole derivatives are an important class of heterocycles, being the core fragment of different natural products and biological systems. The imidazole ring is biologically relevant as it can mimic the histidine moiety. It is able to act as a co-ligand in metal complexes, potentially enabling them to bind with biomolecules [17]. They occupy a unique place in the field of medicinal chemistry owing to their potent biological activity especially as antiprotozoal, antifungal, and antihypertensive agents [18–21]. Bearing donors and acceptors capable of hydrogen bonding, imidazole- and benzimidazole-containing metal complexes often possess interesting supramolecular architectures [22]. In the study of imidazole derivatives, Brandenburg reported that the compound synthesized from Cu(II) with salicylideneanthranilic acid and a co-ligand 2-methylimidazole [Cu(SAA)(MeImH)] had distinct superoxide dismutase activity (SOD) which resulted in 50% inhibition ($IC_{50} = 35$ μmol dm^{-3}) higher than that of the native enzyme ($IC_{50} = 0.004$ μmol dm^{-3}) [23]. This higher IC_{50} value was hypothesized to be due to the strong ligand field created by the tridentate Schiff base that would interfere with the interaction of the complexed copper ion with the superoxide radicals [24].

In the present study, a new series of mixed-ligand metal complexes was formed by reacting single atom donor ligands, imidazole and benzimidazole with tridentate thiosemicarbazide Schiff bases and Ni(II) acetate. Since scarce information has been reported on mixed ligand metal complexes containing imidazole derivatives as a co-ligand and in view of the previous studies on the biological relevance of related mixed-ligand metal complexes, we report herein the synthesis, characterisation, cytotoxicity, antibacterial activity and DNA-binding studies of mixed ligand metal complexes derived from tridentate ONS Schiff bases with imidazole derivatives.

2. Experimental

2.1. Instrumentation and materials

All chemicals were of analytical grade (A.R. from Alfa Aesar, Aldrich or Merck) and used without further purification. Elemental analysis (C, H, N) were performed using a LECO CHNS-932 elemental analyser. Infrared (IR) spectra were recorded on PerkinElmer 100 spectrophotometer (4000-280 cm^{-1}). Molar conductance of 10^{-3} M solutions of the mixed-ligand Ni(II) complexes in DMSO were measured using a Jenway 4310 conductivity meter with a dip-type cell electrode. Magnetic susceptibility was measured with a Sherwood Scientific MSB-AUTO magnetic susceptibility balance at 298 K. UV–Vis spectra were recorded by using a Shimadzu UV-2501 PC recording spectrophotometer in the range of 1000–200 nm. Metal content of the complexes were determined using Inductive Coupled Plasma-Optical Emission Spectrometry. Nuclear Magnetic Resonance (^{1}H NMR and ^{13}C NMR) spectra were recorded using an JNM ECA400 NMR spectrometer.

2.2. Synthesis of 4-methyl-3-thiosemicarbazide-2,4-dihydroxybenzaldehyde (*MT24D*) and 4-phenyl-3-thiosemicarbazide-2,4-dihydroxybenzaldehyde (*PT24D*)

20 mmol (2.76 g) of 2,4-dihydroxybenzaldehyde was dissolved in 30 ml ethanol and added to an equimolar solution of 4-methyl-3-thiosemicarbazide (20 mmol, 2.10 g) or 4-phenyl-3-thiosemicarbazide (20 mmol, 3.34 g) in the same solvent. The mixture was stirred and reduced to half volume from initial volume. The precipitate that formed was recrystallised with cold ethanol. The yields were dried over silica gel overnight.

For **MT24D**. Yield: (86%). Colour: light yellow, melting point: 215–216 °C. Anal. Calc. Data are given in Table 2, IR, ATR ν(cm^{-1}): 3240 ν(O–H), 3336 ν(N–H), 1616 ν(C=N), 1013 ν(N–N), 866 ν(C=S). ^{1}H NMR (400 MHz, DMSO-d_6, δ ppm): 11.41 (s, 1H, NH), 9.45 (q, 1H, $J = 32$ Hz, NH), 8.37 (s, 1H, CH), 8.35 (s, 2H, OH phenolic), 7.33 (d, 1H, $J = 4$ Hz, Ar H), 6.74 (d, 1H, $J = 8$ Hz, Ar H), 6.62 (t, 1H, $J = 24$ Hz, Ar H), 2.45 (d, 3H, $J = 12$ Hz, CH_3). ^{13}C NMR (100 MHz, DMSO-d_6, δ ppm): 177.12 (C8), 146.11 (C5), 144.67 (C3), 140.56 (C7), 121.45 (C6), 118.87 (C4), 116.98 (C1), 116.85 (C2), 31.38 (C9). MS *m/z* 225 (M+1).

For **PT24D**. Yield: (89%). Colour: yellow, melting point: 205–206 °C. Anal. Calc, Data are given in Table 2, IR, ATR ν(cm^{-1}): 3160 ν(O–H), 3240 ν(N–H), 1592 ν(C=N), 1022 ν(N–N), 825 ν(C=S). ^{1}H NMR (400 MHz, DMSO-d_6, δ ppm): 11.71 (s, 1H, NH), 9.96 (s, 1H, OH phenolic), 9.55 (s, 1H, OH phenolic), 8.94 (q, 1H, $J = 32$ Hz, NH), 8.43 (s, 1H, CH), 7.51 (d, 2H, $J = 8$ Hz, Ar H), 7.49 (d, 1H, $J = 12$ Hz, Ar H), 7.33 (t, 2H, $J = 16$ Hz, Ar H), 7.14 (t, 1H, $J = 16$ Hz, Ar H), 6.78 (d, 1H, $J = 16$ Hz, Ar H), 6.64 (t, 1H, $J = 12$ Hz, Ar H). ^{13}C NMR (100 MHz, DMSO-d_6, δ ppm): 176.23 (C8), 146.13 (C5), 145.39 (C3), 141.76 (C7), 139.68 (C9), 128 (C10, C14), 126.23 (C10, C11), 125.57 (C1), 121.54 (C6), 119.40 (C4), 118.59 (C2), 117.20 (C12). MS *m/z* 287 (M+1).

Table 1
Crystal data and refinement details for complexes **2'** and **5**.

Complex	**2′**	**5**
Formula	$C_{16}H_{15}N_5NiO_2S$, $C_7H_6N_2$, CH_4O	$C_{12}H_{14}N_5NiO_2S$, $C_2H_3O_2.2H_2O$
Formula weight	550.28	446.13
Crystal colour	green	brown
Crystal system	Triclinic	Triclinic
Space group	*P*1	*P*1
a/Å	9.9399(6)	7.8339(7)
b/Å	10.4759(7)	10.6523(8)
c/Å	12.0659(7)	11.8297(7)
α/°	99.237(5)	98.363(5)
β/°	93.911(5)	101.635(6)
γ/°	95.581(5)	100.212(7)
V/Å^3	1229.74(13)	934.61(13)
Z	2	2
D_c/g cm^{-3}	1.486	1.585
F(000)	572	464
μ(MoKα)/mm^{-1}	0.915	1.192
Measured data	10943	8119
θ range/°	2.4–25.2	2.4–25.2
Unique data	5562	4206
Observed data ($I \geq 2.0\sigma(I)$)	4207	3531
No. parameters	342	264
R, obs. data; all data	0.045; 0.100	0.042; 0.099
a; *b* in weighting scheme	0.051; 0.257	0.047; 0.550
R_w, obs. data; all data	0.069; 0.112	0.053; 0.106
GoF	1.05	1.04
Range of residual electron density peaks/eÅ^{-3}	−0.40 − 0.57	−0.48 − 0.96

Table 2
Physical properties and elemental analysis of the Schiff bases and mixed-ligand Ni(II) complexes.

Compound (Mol. Wt.)	Color	M.P (°C)	Λ[a]	μ[b] (B.M)	(%) Found (Calcd.)			
					C	H	N	M
MT24D (225.0)	Light yellow	215–216	3.3	–	47.2 (47.9)	5.0 (4.9)	18.6 (18.6)	–
PT24D (287.3)	Yellow	126–127	2.3	–	58.6 (58.5)	4.9 (4.6)	14.7 (14.6)	–
Ni(MT24D)im (**1**) (349.0)	Brown	>300	2.5	Diamagnetic	41.9 (41.2)	4.1 (3.7)	20.7 (20.0)	16.2 (16.7)
Ni(MT24D)bz (**2**) (399.0)	Brown	>300	2.4	Diamagnetic	48.3 (48.0)	4.3 (3.8)	17.8 (17.5)	14.3 (14.6)
Ni(PT24D)im (**3**) (411.0)	Dark brown	>300	2.9	Diamagnetic	50.5 (49.9)	4.0 (3.6)	16.6 (16.9)	14.8 (14.2)
Ni(PT24D)bz (**4**) (461.0)	Brown	>300	3.5	Diamagnetic	54.2 (54.5)	3.9 (3.7)	15.4 (15.1)	12.9 (12.7)

[a] Molar conductance (Ω^{-1} cm^2 mol^{-1}) of 10^{-3} M solutions in DMSO.
[b] Magnetic moments at 298 K.

2.3. Synthesis of mixed-ligand Ni(II) complexes (*1*–*4*)

2 mmol (0.43 g) $Ni(CH_3COO)_2.H_2O$ was dissolved in 20 ml of methanol. 8 mmol (0.54 g) imidazole or benzimidazole (8 mmol, 0.95 g) in 30 ml dichloromethane was added to this solution. The mixture was stirred and heated for about 20 min. A solution of Schiff base, MT24D (2 mmol, 0.45 g) or PT24D (2 mmol, 0.57 g) was added to the metal-imidazole solution. The mixture was heated while stirring to reduce the volume to half. The precipitate formed when the mixture was cooled to room temperature, filtered and dried over silica gel overnight. For imidazole or benzimidazole to remain as a co-ligand, a large excess was added in the reaction.

2.4. Single crystal X-ray structure determination of [Ni(MT24D)(bz)](bz).CH_3OH (*2′*), and the cation of [Ni(MT24D)(im)] $O_2CMe.2H_2O$ (*5*)

In addition to crystals of **2′**, that is **2** co-crystallised with a 1,3-benzimidazole molecule as a methanol solvate, a small number of crystals of a reaction intermediate isolated from the reaction mixture of **1** and characterised crystallographically, hereafter **5**. Intensity data for **2′** and **5** were measured at T = 100 K on an Oxford Diffraction Gemini Eos CCD diffractometer fitted with Mo Kα radiation (λ = 0.71073 Å). Data reduction, including analytical absorption correction, was accomplished with CrysAlisPro [25]. The structures were solved by direct-methods [26] and refined (anisotropic displacement parameters, C-bound H atoms in the riding model approximation) on F^2 [27]. The oxygen and nitrogen-bound hydrogen atoms were located from Fourier difference maps but refined with distance restraints O–H = 0.84 ± 0.01 Å and N–H = 0.88 ± 0.01 Å, respectively. The only exception to this was for the O2w-water-bound hydrogen atoms in **5** which were included in their as-located positions constrained to O–H = 0.83 Å. Even restrained refinement of this water molecule proved unstable, an observation correlated with the relatively large displacement parameters associated with the O2w oxygen atom. A consequence of this is that one of the hydrogen bonds formed by this water molecule is rather weak; it should be noted that the next closest potential acceptor atom for a hydrogen bond is 3.83 Å distant. A weighting scheme $w = 1/[\sigma^2(F_o^2) + (aP)^2 + bP]$ where $P = (F_o^2 + 2F_c^2)/3$) was introduced in each case. In the final cycles of the refinement of **5**, a reflection, i.e. (-6 -4 8), was omitted owing to poor agreement. The molecular structure diagrams was generated with ORTEP for Windows [28] with 70% displacement ellipsoids and the packing diagrams were drawn with DIAMOND [29]. Additional data analysis was made with PLATON [30]. Crystal data and refinement

details are given in Table 1.

2.5. Bioactivity

2.5.1. Cytotoxicity assays

MDA-MB-231 (estrogen receptor-negative human breast cancer cells) and MCF-7 (estrogen receptor-positive human breast cancer cells) cell lines were obtained from the National Cancer Institute, USA. The cells were cultured in tissue culture flasks containing RPMI 1640 culture medium supplemented with 1% penicillin and 10% fetal bovine serum (FBS). The cytotoxicity was determined by using the 3-(4,5-dimethylthiazol-2-yl)-2,5-diphenyltetrazolium bromide (MTT) assay [31]. Cytotoxicity was expressed as IC_{50} which is the concentration of trial compound that inhibits the cancer cells by 50% as compared to the control. The control that contained untreated cells were included for each sample. Tamoxifen was used as a standard drug.

2.5.2. Antibacterial activity

Clinical isolates of the following organisms: Methicillin Resistant *Staphylococcus aureus (MRSA), Staphylococcus aureus, Bacillus subtilis, Serratiamarcescens, Propionibacterium acne, Pseudomonas aeruginosa* and *Enterobacteraerogenes* used in this study were obtained from the culture collection of the Institute of Bioscience, UPM. The bacterial strains were grown and maintained on nutrient agar (NA) slant. Antimicrobial activity was based on a clear zone formed around the disc. Complete inhibition was indicated by a clear zone, while partial inhibition was by a semi-clear zone. Streptomycin (100 mg/mL) was used as the reference drug for antibacterial activity with DMSO as the negative control. The bacterial suspension (10^8 cfu/mL) was inoculated onto the entire surface of a nutrient agar (NA) plate with a sterile cotton-tipped swab to form an even lawn. After solidification, the filter paper discs impregnated with the extracts were placed on the NA plates. The plates were then incubated at 37 °C for 18–24 h. All tests were performed in triplicate and the antibacterial activity was expressed as the mean of the inhibition diameters (mm) obtained.

2.5.2.1. Determination of minimum inhibitory concentration (MIC). The MIC values were determined by the liquid dilution method [32] for samples that displayed inhibition zones of around 15 mm and more in the disc diffusion assay. Various concentrations of each sample (ranging from 0.156 to 20 mg/mL) were prepared in 96-microwell plates followed by inoculating 10 μl of the standardized suspension bacteria. The microwell plates were incubated at 37 °C for 18–24 h. The MICs of the samples were recorded as the lowest concentration that could inhibit the visible growth of microorganisms overnight. Each experiment was carried out three times and was correlated against the controls.

2.5.2.2. Determination of minimum bactericidal concentrations (MBC). A loopful of sample from each well in the MIC examination which did not show any growth was inoculated on NA and incubated at 37 °C for 18–24 h. In this test, the lowest concentration of sample required to kill a particular bacterium was determined as the MBC.

2.5.3. DNA-binding study

The buffer solution was prepared by adding 5 mM Tris-HCl (Sigma Aldrich) and 25 mM NaCl (Sigma Aldrich) in 500 ml ultrapure water (pH = 7.1). The CT-DNA was dissolved in 25 ml of buffer solution [33]. The concentration of CT-DNA was calculated according to Beer-Lambert's Law $A = \varepsilon bc$, where ε is the molar extinction coefficient, 6600 $M^{-1}\,cm^{-1}$ at 260 nm [4]. The calculated DNA concentration was 5.136×10^{-5} M. The complexes were dissolved in a mixture of DMSO/buffer (3:7). Absorption titration measurements were carried out by gradually increasing the DNA concentration while maintaining the complex concentration (2×10^{-6} M). Absorbance values were recorded after each successive addition of DNA solution and equilibration using UV spectrophotometry [34].

3. Results and discussion

Schiff bases (**MT24D** and **PT24D**) were prepared by the condensation reaction of 2,4-dihydroxybenzaldehyde with 4-methyl-3-thiosemicarbazide and 4-phenyl-3-thiosemicarbazide to form uninegatively-charged tridentate Schiff bases. The mixed-ligand Ni(II) complexes (**1**–**4**) were synthesized by reacting Ni(II) acetate, imidazole/benzimidazole (excess) and the Schiff bases in a one-pot reaction. The Schiff bases and mixed-ligand Ni(II) complexes were obtained in good yields with sharp melting points indicating that the compounds were relatively free of impurities. The Schiff bases were soluble in most common organic solvents while the mixed-ligand Ni(II) complexes had limited solubility, and were only completely soluble in DMSO and THF. The physical properties and elemental analyses obtained for the Schiff bases and mixed-ligand Ni(II) complexes are listed in Table 2. All physiochemical and spectroscopic analyses were carried out on the bulk samples.

3.1. Magnetic and conductivity data

All the mixed-ligand Ni(II) complexes exhibited diamagnetic properties which was indicative of d^8 Ni(II) complex with a square planar geometry [3] since the Schiff bases were expected to coordinate with the metal atom through three donor atoms while imidazole or benzimidazole occupied the fourth position. The complexes were non-electrolytes in DMSO [35], which fell in the range of 2.3–3.3 $\Omega^{-1}\,cm^2\,mol^{-1}$, indicating that both imidazole/benzimidazole and ligand did not exist as free ions in solution.

3.2. Electronic and IR spectra

The infrared spectral data for the ligand and metal complexes are shown in Table 3 and Figs. S1, S2 and S3 (Supplementary file). Both ligands successfully coordinated to the metal ion through the phenoxide-oxygen, azomethine-nitrogen, and thiolate-sulphur atoms as evidenced by shift of wavenumbers of certain key functional groups in the IR spectra. The absence of the *ν*(S–H) band at 2570 cm^{-1} in the spectra of the ligands indicated that they existed as the thione form in the solid-state [34]. The thione forms are unstable and tend to convert to stable thiolo forms in the presence of metal ions, by enethiolization in solution [36]. In the infrared spectrum of MT24D and PT24D ligands, strong bands were observed at 1616 cm^{-1} and 1592 cm^{-1} respectively, representing *ν*(C=N) and these bands shifted to lower wavenumbers indicating

Table 3
IR spectral bands of the Schiff bases and their mixed-ligand Ni (II) complexes.

Compound	*ν* (O–H)	*ν* (N–H)	*ν* (C=N)[a,b]	*ν* (N–N)	*ν* (C=S)	*ν* (C–S)
MT24D	3240	3336	1616	1013	866	–
PT24D	3160	3240	1592	1022	825	–
1	3076	3383	1600, 1670	1071	–	732
2	3095	3394	1594, 1748	1130	–	737
3	3049	3362	1596, 1699	1022	–	742
4	3162	3353	1593, 1700	1121	–	740

[a] C=N from ligand.
[b] C=N from imidazole/benzimidazole.

that the metal ions coordinated through the azomethine-nitrogen. A weak ν(C=N) band from imidazole or benzimidazole appeared in the region 1699-1748 cm^{-1} indicative of their presence as a co-ligand. A broad ν(O–H) band was seen in the region of 3049–3240 cm^{-1} for both ligands and complexes. ν(C=S) band appeared in the ligands at 866 cm^{-1} and 825 cm^{-1} for MT24D and PT24D respectively and shifted to lower wavenumbers upon complexation of the ligands and Ni(II) ion in the region of 732–742 cm^{-1}.

The electronic spectral analysis was carried out in DMSO and the data is displayed in Table 4. The bands at 261–280 and 300–353 nm were attributed to intra-ligand n-π^* and π-π^* transitions respectively [37]. Weak *d-d* transitions displayed at 400–500 nm indicated that the complexes had square planar geometry where the Ni(II) ion was coordinated to the azomethine-nitrogen, hydroxyl-oxygen, thiolate-sulphur from the Schiff base, whereas the fourth position was occupied by the co-ligand, imidazole or benzimidazole. The appearance of a strong peak at 347–377 nm additionally supported the ligation of sulphur to the metal ion via ligand to metal charge-transfer transitions.

3.3. ^{1}H NMR and ^{13}C NMR spectra

To obtain insight and confirm the structure of the tridentate Schiff bases, ^{1}H NMR spectra of MT24D and PT24D (Figs. S4 and S5, Supplementary Data) in DMSO-d_6 were obtained. The summary of the spectral data is shown in Tables S1 and S2 (Supplementary Data). The ^{1}H spectra MT24D showed a resonance in the downfield region around δ 11 ppm which was assigned as the proton (H7) which was attached to the N atom. The existence of the electronegative atoms (nitrogen) adjacent this proton deshields the proton. One singlet at δ 8.35 and two singlets at δ 9.55 and 9.96 ppm were observed correspond to OH phenolic of MT24D and PT24D, respectively. The aromatic protons were observed as multiplet ranging δ 6.62–7.33 ppm corresponding to 3 protons and δ 6.64–7.51 ppm corresponding to 8 protons for MT24D and PT24D, respectively. No resonance was observed at δ 4.0 ppm which indicated the absence of the thiol group which proved that the Schiff bases were present in their thione tautomeric form in solution [38].

The ^{13}C{^{1}H} NMR spectra and Distortionless Enhancement by Polarization Transfer (DEPT) experiments (Figs. S6 and S7, Supplementary Data) were used to identify and assign the carbon atoms of the Schiff bases. The summary of the spectral data of MT24D and PT24D is shown in Table S2 (Supplementary Data). The signal due to the methyl group was observed at δ 31.38 ppm. The thiocarbonyl group (–C=S) was assigned at the region δ 176.23–177.12 ppm in the most deshielded regions. All the other aromatic carbon shifts were observed in the region of δ 116.85–128.69 ppm [15].

3.4. Crystal structures of [Ni(MT24D)(bz)].CH_3OH (**2′**) and [Ni(MT24D)(im)]$O_2CMe.2H_2O$ (**5**)

Crystal structure determinations were achieved for **2′** and **5** with the molecular structures of each of the complex molecules shown in Fig. 1. The crystallographic asymmetric unit of **2′** comprises a neutral complex molecule, a 1,3-benzimidazole molecule and a solvent methanol molecule. The tridentate di-anion coordinates the nickel(II) centre via thiolate-S1, phenoxide-O3 and imine-N3 atoms to establish five- and six-membered rings. The fourth site of the central atom is occupied by the N4 atom derived from a neutral benzimidazole molecule. The nitrogen atoms are mutually *trans* within the resultant N_2OS donor set that defines an approximate square-planar geometry. Selected geometric data are given in Table 5 from which it can be seen that the maximum deviation from the ideal geometry, at least in terms of angles is found in the O1–Ni–N3 angle of 95.69(8)°.

The crystallographic asymmetric unit of **5** comprises a complex cation, an acetate anion and two water molecules of crystallisation. The tridentate mono-anion coordinates the nickel(II) centre via thione-S1, phenoxide-O3 and imine-N3 atoms. The fourth site of the central atom is occupied by the N4 atom derived from a neutral imidazole molecule. A very similar description of the coordination geometry pertains to the complex cation in **5** with the key

Table 4
Electronic absorption bands of the Schiff bases and their mixed-ligand Ni (II) complexes.

Compound	Electronic spectra (in DMSO) λ_{max}(log ε)^c
MT24D	280 (3.08); 348 (4.37)
PT24D	279 (4.11); 353 (2.41)
1	261 (4.80); 301 (3.92); 365 (4.13); 406 (3.99)
2	279 (4.81); 300 (3.93); 369 (4.09); 404 (3.95)
3	270 (6.43); 304 (6.48); 347 (6.54); 406 (7.61)
4	280 (4.87); 308 (4.13); 377 (4.23); 411 (4.17)

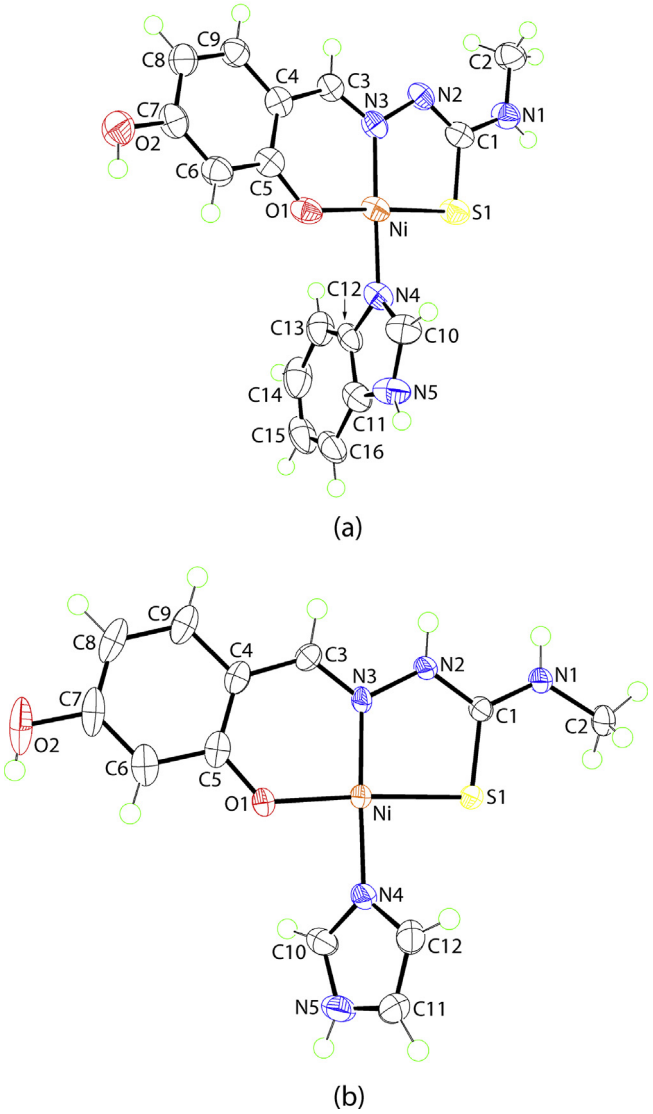

Fig. 1. Molecular structures of the complex molecules in (a) **2′** and (b) **5**, showing atom labelling schemes.

Table 5
Selected geometric parameters (Å, °) for **2′** and **5**.

Complex	2′	5
Parameter		
Ni–S1	2.1365(8)	2.1545(7)
Ni–O1	1.8799(18)	1.8597(17)
Ni–N3	1.862(2)	1.853(2)
Ni–N4	1.897(2)	1.894(2)
N2–N3	1.417(3)	1.397(3)
C1–S1	1.744(2)	1.715(2)
C1–N1	1.350(3)	1.326(3)
C1–N2	1.308(3)	1.453(3)
C3–N3	1.304(3)	1.301(3)
S1–Ni–O1	174.82(6)	176.43(6)
S1–Ni–N3	87.54(7)	88.60(6)
S1–Ni–N4	89.95(7)	89.25(7)
O1–Ni–N3	95.69(8)	94.90(8)
O1–Ni–N4	86.94(8)	87.26(8)
N3–Ni–N4	176.94(9)	177.47(9)
C1–N2–N3	111.4(2)	117.4(2)
N2–N3–C3	113.2(2)	115.2(2)
S1–C1–N1	117.7(2)	122.78(19)
S1–C1–N2	122.8(2)	118.61(19)
N1–C1–N2	119.4(2)	118.6(2)

difference being the thiolate-S1 donor in **2′** is now a thione-S1 atom as the tridentate ligand is a mono-anion. The major angular deviation from the square-planar N_2OS coordination geometry is again seen in the O1–Ni–N3 angle of 94.90(8)°. The experimental equivalence of the C13–O3, O4 bond lengths, i.e. 1.244(4) and 1.249(3) Å, respectively, confirms the presence of the acetate counter-ion in the crystal of **5**.

Systematic changes in key geometric parameters are evident in Table 5, as a result of the different coordination modes of the LH^- and L^{2-} anions in **5** and **2′**, respectively. Most notable is the longer Ni–S1 bond length in **5** compared with that in **2′**, with concomitant differences in the Ni–O1 bond lengths. The short C1–S1 bond length in **5** is also consistent with the presence of a thione-S1 atom. Also, the C1–N2 length of 1.308(3) Å in **2′** is consistent with the formation of an imine bond in the L^{2-} di-anion. This change is also reflected in some of the key angles, e.g. a reduction of ca 6° in the C1–N2–N3 angle, and a decrease and increase by 5° and 4° in the S1–C1–N1 and S1–C1–N2 angles, respectively going from **5** to **2'**.

The tridentate mode of coordination of the L^{2-} and LH^- anions in **2′** and **5** results in the formation of five-membered Ni,S1,C1,N2,N3 and six-membered Ni,O1,N3,C3–C5 chelate rings. While essentially planar, there are significant deviations from planarity in the five-membered ring of **2'**: the r.m.s. deviation = 0.0210 Å with the N3 atom deviating by 0.0290(12) Å from this plane. Even more pronounced are the deviations in the six-membered chelate ring with the r.m.s. deviation for the fitted atoms being 0.0459 Å, and with the N3 and Ni atoms lying 0.0723(14) and 0.0559(10) Å to either side of the plane, respectively; the dihedral angle between the chelate rings = 6.19(10)°. Another description for the conformation of the six-membered chelate ring is one based on an envelope with the Ni atom being the flap atom, lying 0.152(3) Å out of the plane defined by the remaining five atoms [r.m.s. deviation = 0.0288 Å]. The coordinated 1,3-benzimidazole molecule [r.m.s. deviation = 0.0125 Å] occupies a position almost perpendicular to the tridentate ligand as seen in the dihedral of 88.94(6)° formed between it and the five-membered chelate ring. The non-coordinating 1,3-benzimidazole molecule is also planar [r.m.s. deviation = 0.0125 Å]. A difference in conformation in the chelate rings is evident in **5**. In **5**, both rings are planar with the greatest deviation from the five-membered ring [r.m.s. deviation = 0.0091] being 0.0137(12) Å for the N3 atom. The equivalent parameters for the larger chelate ring are 0.0108 Å and 0.0151(17) Å for the C5 atom. The dihedral angle between the chelate rings is 0.861(9)°. The imidazole ring is inclined with respect to the rest of the molecule as seen in the dihedral angle of 50.69(7)° it forms with the five-membered chelate ring.

The other obvious difference in conformation between the complex molecules in **2′** and **5** relates to the relative orientations of the terminal amine-bound methyl groups. While in both molecules, this group is co-planar with the coordinated S1 atom with S1–C1–N1–C2 torsion angles of and 171.5(2) and −1.87(16)° in **2** and **5**, respectively, in **5**, the methyl group is syn to the S1 atom whereas there is an anti-relationship in **2'**.

The mode of coordination of the LH^- anion in **5** appears to be unprecedented in the crystallographic literature according to a search of the Cambridge Structural Database [39]. Similarly, with a formal C3–C4 bond in **2′**, this is also unprecedented with the closest structural analogue being a nickel(II) complex where this bond is substituted by a bond of an aromatic ring [40].

As anticipated from the chemical compositions of **2′** and **5**, significant hydrogen bonding interactions are evident in their crystals. The geometric parameters characterising these along with other non-covalent interactions present in the respective crystals are tabulated in Table 6.

Hydrogen bonding interactions also feature prominently in the molecular packing of **2'**. The hydroxyl group of the complex molecule forms a hydroxyl-O–H···N(benzimidazole) hydrogen bond with a lattice benzimidazole molecule which, in turn, forms a benzimidazole-N–H···O(methanol) hydrogen bond. The solvent molecule functions in the same way by forming methanol-O–H···N(imine) and coordinated-benzimidazole-N–H···O(methanol) hydrogen bonds. The result is a supramolecular chain along the c-axis direction as shown in Fig. 2(a). While there is no role formal role for the amine-N–H hydrogen in the hydrogen bonding scheme, this atom participates in the molecular packing by forming in a N–H ··· π(C_6-benzimidazole) interaction within the supramolecular chain as detailed in Fig. 2(b). The chains are connected into a supramolecular layer in the bc-plane by π ··· π stacking interactions between symmetry related benzimidazole rings, i.e. (N4,N5,C10–C12) and $(C11–C16)^i$ rings with an inter-centroid separation of 3.6142(16) Å and angle of inclination = 1.23(14)°; symmetry operation (i): 2-x, 2-y, 1-z. Layers stack along the a-axis direction without directional interactions between them, Fig. 2(c).

In the crystal of **5**, the acetate anion spans the two amine-N–H

Table 6
Geometric parameters (Å, °) characterising intermolecular interactions in the crystals of **2′** and **5**.[a]

A	H	B	H···B	A ... B	A-H...B	Symmetry operation
2′						
O2	H2o	N6	1.90(3)	2.741(3)	172(3)	1-x, 1-y, -z
O3	H3o	N2	1.982(13)	2.805(3)	164(4)	1-x, 1-y, 1-z
N5	H5n	O3	1.927(14)	2.804(3)	175(3)	1 + x, y, z
N7	H7n	O1	1.96(3)	2.833(3)	169(3)	−1+x, y, z
N1	H1n	Cg(1)	2.68(2)	3.480(2)	153.7(18)	1 + x, y, 1 + z
5						
N1	H1n	O3	1.937(18)	2.808(3)	173(3)	1-x, 1-y, 1-z
N2	H2n	O4	1.842(17)	2.718(3)	176(3)	1-x, 1-y, 1-z
O2	H2o	O2w	1.99(2)	2.825(4)	172(3)	x, y, z
N5	H5n	O1w	1.90(2)	2.759(3)	167(3)	-x, 1-y, -z
O1w	H1w	O1	2.01(3)	2.852(3)	177(3)	x, y, z
O1w	H2w	O4	1.93(3)	2.763(3)	171(3)	x, y, z
O2w	H3w	O3	1.96	2.678(5)	145	1-x, -y, -z
O2w	H4w	O4	2.67	3.438(4)	154	x, y, z

[a] Cg(1) is the ring centroid of the C18–C23 ring.

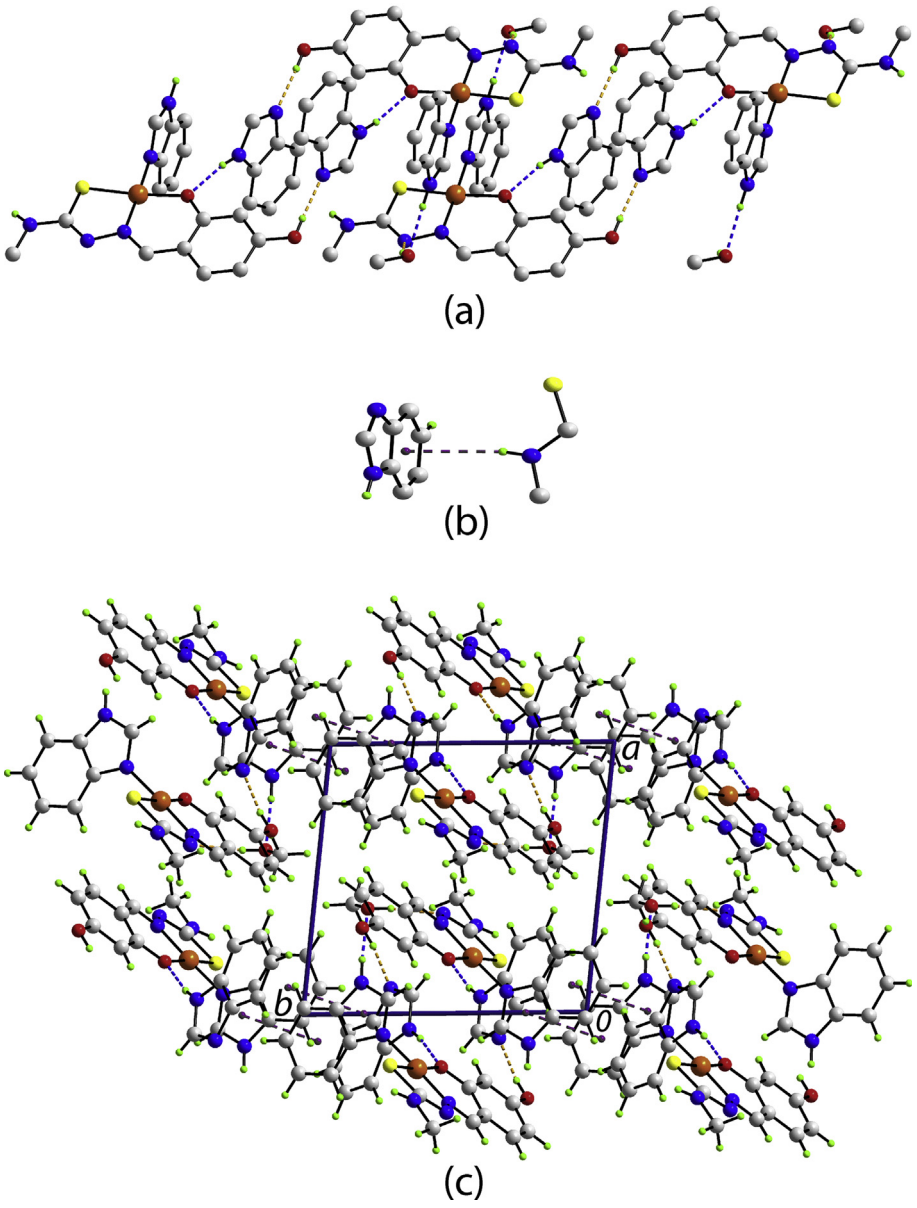

Fig. 2. Supramolecular association in the crystal of **2**: (a) a view of the supramolecular chain along the c-axis direction and sustained by O—H···N and N—H···O hydrogen bonding shown as orange and blue dashed lines, respectively, (b) detail of the amine-N—H ··· π interaction highlighted as a purple dashed line and (c) a view in projection down the c-axis of the unit cell contents of **1** with π ··· π interactions shown as purple dashed lines.

atoms via two charge-assisted amine-N—H…O(carboxylate) hydrogen bonds to form an eight-membered {···OCO···HNCNH} heterosynthon. The presence of hydroxyl-O—H···O2w(water), imidazole-N—H···O1w(water) and water-O1w ··· O2(phenoxide) hydrogen bond provide further links between the complex cation and the other constituents of the crystal. Each of the carboxylate-O atoms forms a water-O-H···O(carboxylate) hydrogen bond, derived from different water molecules. Finally, the H4w atom participates in a long hydrogen bond with the carboxylate-O4 atom. A view of the unit cell contents is shown in Fig. 3. From here, globally, complex cations stack along the crystallographic a-axis and are connected into a three-dimensional architecture via the aforementioned hydrogen bonds which extend laterally from the columns.

4. Biological activities

4.1. Cytotoxic activities

The Schiff bases and the mixed-ligand Ni(II) complexes were screened against two breast cancer cell lines, MCF-7 (positive estrogen receptor human breast cancer) and MDA-MB-231 (negative estrogen receptor human breast cancer). The IC_{50} values (concentration of drug that inhibits the growth of cancer cells by 50% as compared to the untreated controls) were determined. An IC_{50} value of less than 0.5 μM indicates that the complex is strongly active, whereas IC_{50} values of 0.5—5.0 μM and more than 5.0 μM indicate that the complex is moderately active and inactive, respectively [41]. All the compounds were inactive against the tested cancer cell lines. This could have been due to the presence of a hydroxyl group in the Schiff bases of Ni(II) complexes that

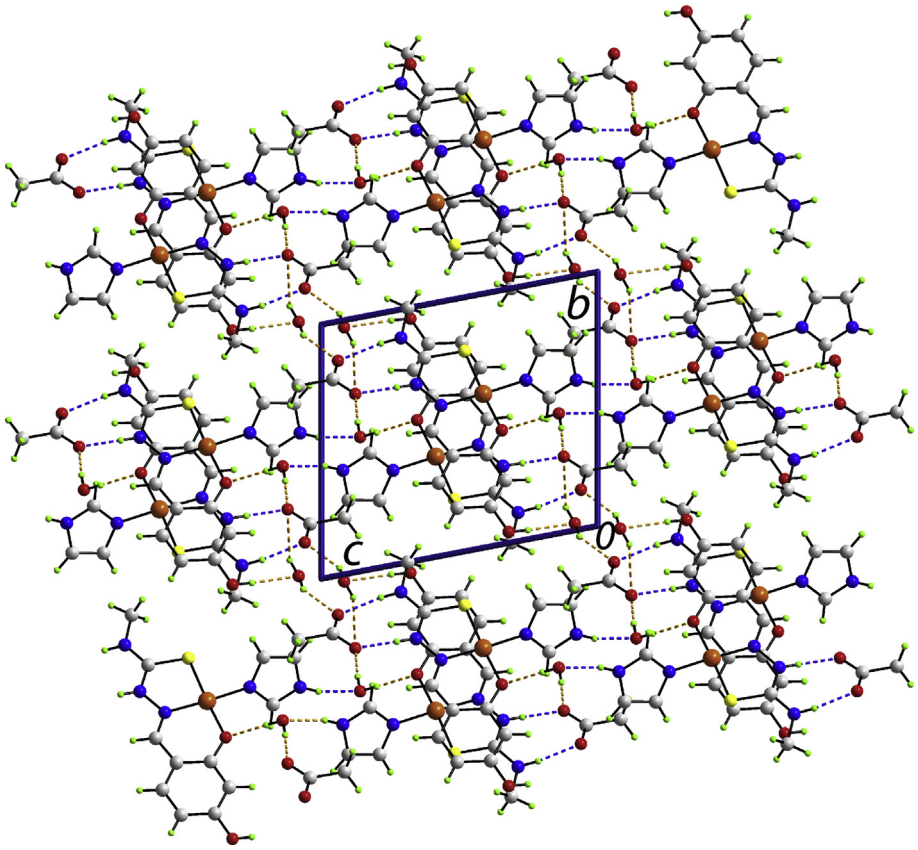

Fig. 3. A view in projection down the a-axis of the unit cell contents of **5**. The O—H···O and N—H···O hydrogen bonds are shown as orange and blue dashed lines, respectively.

reduced the cytotoxicity, probably due to greater steric hindrance and intramolecular H-bonding between the compounds [42]. Interestingly, the PT24D and Ni(II) complexes were observed to have antibacterial potency against the bacterial strains tested.

4.2. Antibacterial activities

The Schiff bases, and mixed-ligand Ni(II) complexes were screened for their antibacterial properties against *Staphylococcus aureus, Bacillus subtilis, Propionibacterium acne* (Gram-positive), and *Pseudomonas aeruginosa, Serratiamarcescens, Enterobacteraerogenes* (Gram-negative). Streptomycin was used as a positive control and DMSO was used as negative control. The disc diffusion assay data is tabulated in Table 7 while the minimum inhibition concentration (MIC) and minimum bacterial concentration (MBC) results are recorded in Table 8.

The mixed-ligand Ni(II) complexes were observed to have better antibacterial activity as compared to the Schiff bases suggesting that the metal ions reduced the polarity of the compounds through the partial sharing of positive charge with the donor atoms of Schiff bases [43]. Hence, π-electron delocalisation upon chelation which also increased the lipophilic character of the central metal atom allowed the Ni(II) complexes to have a stronger permeating ability to enter the permeable membrane of the bacterial strains [44]. This was also observed in similar mixed-ligand Ni(II) complexes with sap (salicylidene-2-aminophenol) and imidazole which had significant antibacterial activities compared to other Ni(II) complexes containing only 2-carboxybenzaldehyde thiosemicarbazone [45,46]. The complexes in this study seemed to be more bacteriocidal towards the gram-positive bacteria tested. Complex **2** had the smallest MIC and MBC values against Pseudomonas Aeruginosa whereas **1** had small MIC and MBC values against a range of both positive and negative gram bacteria, suggesting that only small amounts of the metal complex were required to inhibit/kill the

Table 7
Disc diffusion assay of the Schiff bases and mixed-ligand Ni(II) complexes against selected bacterial strains.

Sample (20 mg/mL)	Gram-positive bacteria				Gram-negative bacteria		
	Staphylococcus aureus	*Bacillus subtilis*	*Propionibacterium acne*	MRSA	*Pseudomonas aeruginosa*	*Serratiamarcescens*	*Enterobacteraerogenes*
MT24D	0	0	0	0	0	0	0
1	19 ± 2	14 ± 1	17 ± 3	0	0	7 ± 1	0
2	17 ± 2	13 ± 1	18 ± 1	0	0	0	0
PT24D	12 ± 2	10 ± 1	14 ± 1	10 ± 1	0	9 ± 1	14 ± 1
3	0	0	0	0	0	11 ± 1	0
4	13 ± 2	11 ± 1	13 ± 1	0	0	0	10 ± 0
Streptomycin	24 ± 2	29 ± 0	19 ± 0	28 ± 3	26 ± 1	21 ± 1	25 ± 1

[a] Diameter of **15 mm** and above is considered active; 0, inactive.

Table 8
Results of minimum inhibitory concentration (MIC) and minimum bactericidal concentration (MBC). (results are in mg/mL).

Sample	*Staphylococcus aureus*		*Bacillus subtilis*		*Propionibacterium acne*		*Enterobacteraerogenes*	
	MIC	MBC	MIC	MBC	MIC	MBC	MIC	MBC
1	0.63	1.25	10.0	20.0	0.63	1.25	–	–
2	1.25	2.50	–	–	0.16	0.31	–	–
PT24D	–	–	–	–	–	–	10.0	20.0
4	10.0	20.0	–	–	–	–	–	–

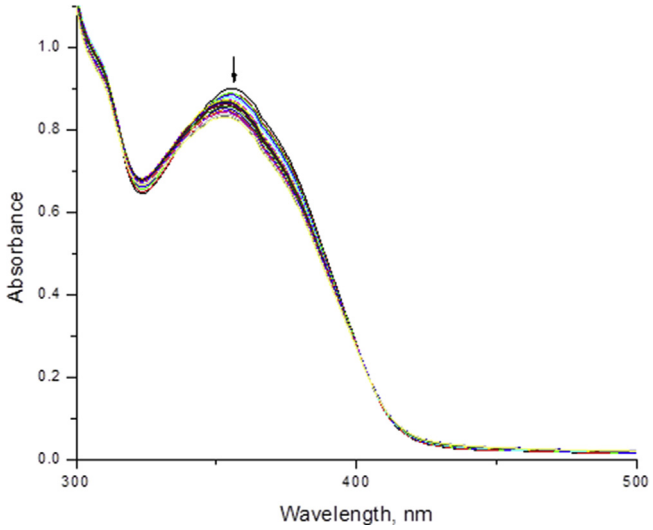

Fig. 4. Electronic spectra of **1** in Tris-HCl buffer upon addition of CT-DNA. The arrow shows the emission intensity changes upon increasing DNA concentration from 0 μL DNA to 240 μL DNA.

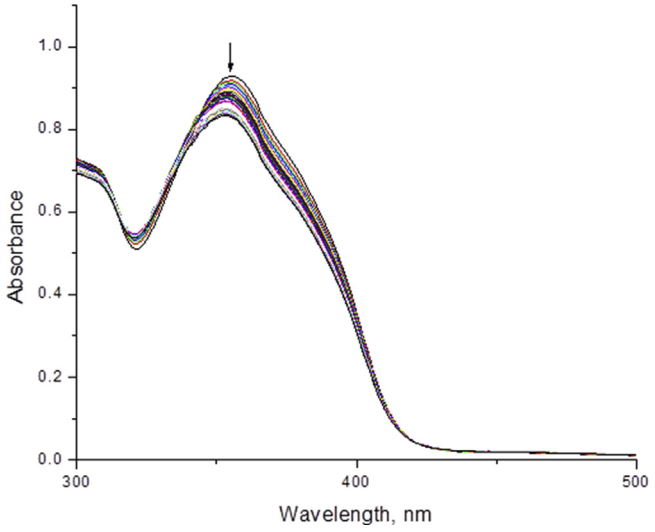

Fig. 5. Electronic spectra of **2** in Tris-HCl buffer upon addition of CT-DNA. The arrow shows the emission intensity changes upon increasing DNA concentration from 0 μL DNA to 240 μL DNA.

growth of the micro-organism [47].

4.3. DNA-binding studies

Electronic absorption spectroscopy is a universal technique used to investigate the strength and mode of binding interactions between compounds **1** and **2** with CT-DNA [4]. The UV spectra of **1** and **2** in the absence and presence of CT-DNA is given in Figs. 4 and 5, respectively. Both spectra exhibited hypochromism of 17.2% and 23.4% for **1** and **2**, respectively indicating that the π orbital of aromatic chromophore of the complexes interacted with π orbital of nucleobases of DNA [48]. The intrinsic binding constant K_b of the complex with CT-DNA was determined according to the following equation [4]:

$$[DNA] \Big/ (\varepsilon_a - \varepsilon_f) = [DNA] \Big/ (\varepsilon_b - \varepsilon_f) + 1/K_b(\varepsilon_b - \varepsilon_f),$$

where [DNA] is the concentration of DNA in the base pairs, K_b is the intrinsic binding constant, ε_a corresponds to the apparent extinction coefficient, and ε_b and ε_f correspond to the extinction coefficients of the bound and free forms of the complex, respectively. The K_b value obtained for **1** was $4.2 \times 10^2\ M^{-1}$ while for **2** it was $5.7 \times 10^3\ M^{-1}$ which was high, an indication of strong and stable interactions between the complexes and CT-DNA [49,50]. Comparing the molecular structures of both the complexes, it was expected that the greater number of coplanar aromatic rings in the latter could have led to a higher affinity for DNA [51]. The interaction between **2** and DNA was also better than **1** possibly due to the presence of aromatic benzimidazole rings where the nitrogen atom of benzimidazole interacted well with the nucleobases of DNA. However, despite good K_b values, both complexes had weaker interactions as compared to the interaction of the standard, ethidium bromide with the DNA base pairs (K_b: $7 \times 10^7\ M^{-1}$) [52].

5. Conclusions

The reaction of Ni(II) acetate with Schiff bases derived from 4-substituted-3-thiosemicarbazide and 2,4-dihydroxybenzaldehyde in the presence of imidazole or benzimidazole yielded a new series of mixed-ligand Ni(II) complexes, **1**–**4**. The Schiff bases coordinated to the Ni(II) ion via deprotonated ONS donor atoms and a monodentate nitrogen atom from imidazole or benzimidazole, yielding a distorted square planar geometry as was supported by spectroscopic analysis. Indirect evidence for the proposed structures were provided by crystallographic methods. X-ray crystallography established the complex in **2′** and complex cation in **5** to exist within trans-N_2OS square planar coordination geometry. In **5**, the sulphur atom is a thione as opposed to a thiolate in **2'**. The form (charge) of the tridentate ligand gave rise to systematic changes in bond lengths and angles. Considerable hydrogen bonding led to a three-dimensional architecture in the crystal of **5** but, only one-dimensional chains in **2'**. All the tested compounds were inactive against the two selected breast cancer cell lines. Although the complexes had higher activity than their free Schiff bases against the tested microbes, their K_b values were significantly lower than

the standard, indicating that the complexes had a different mode of action against the tested cancer cells and microbes in this work.

Acknowledgements

We thank the Faculty of Science, the Faculty of Medicine and Health Science at Universiti Putra Malaysia (UPM) and the Institute of Bioscience, Universiti Putra Malaysia for the provision of laboratory facilities. The research was funded by UPM under University Grant Scheme (IPS 9548700 and IPB 9581001) and the Malaysian Fundamental Research Grant Scheme (FRGS No. 5524940).

Appendix A. Supplementary data

Supplementary data to this article can be found online at https://doi.org/10.1016/j.molstruc.2019.126888.

References

[1] P. Krishnamoorthy, P. Sathyadevi, A.H. Cowley, R.R. Butorac, N. Dharmaraj, Eur. J. Med. Chem. 46 (2011) 3376–3387.
[2] F. Arjmand, A. Jamsheera, D.K. Mohapatra, J. Photochem. Photobiol., A 121B (2013) 75–85.
[3] R.P. Bonomo, E. Conte, G. De Guidi, G. Maccarrone, E. Rizzarelli, G.J. Vecchio, J. Chem. Soc. Dalton Trans. 23 (1996) 4351–4355.
[4] X. Li, C.F. Bi, Y.H. Fan, X. Zhang, X.D. Wei, X.M. Meng, Transit. Met. Chem. 39 (2014) 577–584.
[5] J. Haribabu, K. Jeyalakshmi, Y. Arun, N.S.P. Bhuvanesh, P.T. Perumal, R. Karvembu, J. Biol. Inorg. Chem. 22 (2017) 461–480.
[6] M.M. Tamizh, B.F.T. Cooper, C.L.B. Macdonald, R. Karvembu, Inorg. Chim. Acta (2013) 391–394.
[7] M. Kalita, T. Bhattacharjee, P. Gogoi, P. Barman, R.D. Kalita, B. Sarma, S. Karmakar, Polyhedron 60 (2013) 47–53.
[8] Z.A. Kaplancıklı, M.D. Altıntop, B. Sever, Z. Cantürk, A. Özdemir, J. Chem. (2016) 1–7. ID 1692540.
[9] M. Serda, D.S. Kalinowski, N. Rasko, E. Potůčková, A. Mrozek-Wilczkiewicz, R. Musiol, PLoS One 9 (2014), e110291.
[10] K.C. Park, L. Fouani, P.J. Jansson, D. Wooi, S. Sahni, D.J.R. Lane, D.R. Richardson, Metall 8 (2016) 874–886.
[11] P.F. Salas, C. Herrmann, C. Orvig, Chem. Rev. 113 (2013) 3450–3492.
[12] S. Kathiresan, S. Mugesh, J. Annaraj, M. Murugan, New J. Chem. 41 (2017) 1267–1283.
[13] M. Abid, S.M. Agarwal, A. Azam, Eur. J. Med. Chem. 43 (2008) 2035–2039.
[14] V. Mahalingam, N. Chitrapriya, F.R. Fronczek, K. Natarajan, Polyhedron 27 (2008) 2743–2750.
[15] I. Dilovic, M. Rubcic, V. Vrdoljak, S.K. Pavelic, M. Kralj, C.I.M. Piantanida, Bioorg. Med. Chem. 16 (2008) 5189–5198.
[16] N.A. Mazlan, T.B.S. Ravoof, E.R.T. Tiekink, M.I.M. Tahir, A. Veerakumarasivam, K.A. Crouse, Trans. Met. Chem. 39 (6) (2014) 633–639.
[17] M. Heijden, P.M.V. Vliet, J.G. Haasnoot, J. Reedijk, Dalton Trans. 24 (1993) 3675–3679.
[18] A. Puratchikody, M. Doble, Bioorg. Med. Chem. 15 (2007) 1083–1090.
[19] F. Bellina, S. Cauteruccio, R. Rossi, Tetrahedron 63 (2007) 4571–4624.
[20] R. Di Santo, A. Taf, R. Costi, J. Med. Chem. 48 (2005) 5140–5153.
[21] S. Dutta, Acta Pharm. 60 (2010) 229–235.
[22] D.M.L. Goodgame, M. Goodgame, G.W. Rayner-Canham, Inorg. Chim. Acta 3 (1969) 406–410.
[23] K. Brandenburg, Diamond, Crystal Impact, GbR, Bonn, 2006.
[24] T.B.S. A Ravoof, K.A. Crouse, M.I.M. Tahir, A.R. Cowley, M.A. Ali, Polyhedron 23 (16) (2004) 2491–2498.
[25] Agilent Technologiers, CrysAlis PRO, Agilent Technologies Inc., 2011.
[26] G.M. Sheldrick, A short history of SHELX, Acta Crystallogr. Sect. A Found. Crystallogr. 64 (2008) 112–122.
[27] G.M. Sheldrick, Crystal structure refinement with SHELXL, Acta Crystallogr. Sect. C Struct. Chem. 71 (2015) 3–8.
[28] L.J. Farrugia, WinGX and ORTEP for Windows: an update, J. Appl. Crystallogr. 45 (2012) 849–854.
[29] K. Brandenburg, DIAMOND, Crystal Impact GbR, 2006.
[30] A.L. Spek, Acta Crystallogr. Sect. D Biol. Crystallogr. 65 (2009) 148–155.
[31] T. Mosmann, J. Immunol. Methods (1983) 65–72.
[32] M. Balouiri, M. Sadiki, S.K. Ibnsouda, J. Pharm. Anal. 6 (2016) 71–79.
[33] Y. Wang, J.W. Mao, C. Ding, Z.Q. Pan, J.F. Li, H. Zhou, Transit. Met. Chem. 39 (2014) 111–118.
[34] M.A. Ali, M.T.H. Tarafder, J. Inorg. Nucl. Chem. 39 (1977) 1785–1791.
[35] K. Mounika, B. Anupama, J. Pragathi, C. Gyanakumari, J. Sci. Res. 2 (3) (2010) 513–524.
[36] J.R. Dilworth, R. Hueting, Inorg. Chim. Acta 389 (2012) 389–392.
[37] R.N. Patel, V.L.N. Gundla, D.K. Patel, Polyhedron 27 (2008) 1054–1060.
[38] V. Vrdoljak, M. Cindric, D. Milic, D. Matkovic-Calogovic, P. Novak, B. Kamenar, Polyhedron 24 (2005) 1717–1726.
[39] C.R. Groom, I.J. Bruno, M.P. Lightfoot, S.C. Ward, S.C., The Cambridge structural database, Acta Crystallogr. Sect. B Struct. Sci. Cryst. Eng. Mater. 72 (2016) 171–179.
[40] Z. Afrasiabi, P. Stovall, K. Finley, A. Choudhury, C. Barnes, A. Ahmad, F. Sarkar, A. Vyas, S. Padhye, Spectrochim. Acta, Part A 114 (2013) 114–119.
[41] C.K. Chah, T.B.S.A. Ravoof, A. Veerakumarasivam, Pertanika J. Sci. Technol. 26 (2018) 653–670.
[42] J.V. Duncia, J.B. Santella, C.A. Higley, W.J. Pitts, J. Wityak, W.E. Frietze, R.E. Olson, Bioorg. Med. Chem. Lett 8 (1998) 2839–2844.
[43] K. Singh, R. Thakur, V. Kumar, J. Basic Appl. Sci. 5 (2016) 21–30.
[44] E. Ispir, Dyes Pigments 82 (2009) 13–19.
[45] M. Salehi, F. Rahimifar, M. Kubicki, A. Asadi, Inorg. Chim. Acta 443 (2016) 28–35.
[46] S. Chandra, Vandana, Spectrochim. Acta A Mol. Biomol. Spectrosc. 129 (2014) 333–338.
[47] M.R. Mlahi, O.A. El-Gammal, M.H. Abdel-Rhman, I.M. AbdAl-Gader, J. Mol. Struct. 1182 (2019) 168–180.
[48] X. Wang, Y. Du, L. Fan, H. Liu, Y. Hu, Polym. Bull. 55 (2005) 105–113.
[49] S. Arounaguiri, D. Easwaramoorthy, A. Ashokkumar, A. Dattagupta, B.G. Maiya, J. Chem. Sci. 112 (2000) 1–17.
[50] S. Mathur, S. Tabassum, Cent. Eur. J. Chem. 4 (2006) 502–522.
[51] H. Wu, F. Shi, X. Wang, Y. Zhang, Y. Bai, J. Kong, C. Wang, Transit. Met. Chem. 39 (2014) 261–270.
[52] M.J. Waring, J. Mol. Biol. 13 (1965) 269–282.